3.10. Accuracy in Rietveld quantitative phase analysis with strictly monochromatic Mo and Cu radiations

L. León-Reina, A. Cuesta, M. García-Maté, G. Álvarez-Pinazo, I. Santacruz, O. Vallcorba, A. G. De la Torre and M. A. G. Aranda

3.10.1. Introduction

Most industrial materials are multiphase systems and the accurate determination of their phase assemblage is key to understanding their performances. There are different approaches to carrying out quantitative phase analysis (QPA; see Chapter 3.9); however, nowadays, the Rietveld method is the most widely employed methodology for QPA of crystalline materials (Madsen *et al.*, 2001; Scarlett *et al.*, 2002), including cements (Stutzman, 2005; León-Reina *et al.*, 2009; Chapter 7.12).

The factors affecting the accuracy and precision of Rietveld quantitative phase analysis (RQPA) results can be gathered into three main groups: (i) instrument related, (ii) sample-preparation related and (iii) data-analysis protocol(s). The Rietveld method is a standardless methodology which uses the crystal-structure descriptions of each crystalline component to calculate its powder pattern. For this reason, the correct choice of crystal-structure description for each phase in multiphase materials is key (Zevin & Kimmel, 1995; Madsen *et al.*, 2001, 2011). The influence of the instrument type on RQPA has previously been evaluated (Madsen *et al.*, 2001) and the main conclusion was that neutron and synchrotron powder diffraction yielded the best results owing to larger irradiated volumes and also to the minimization of microabsorption effects.

High-energy (short-wavelength) X-rays contribute (i) to minimize absorption and microabsorption effects, (ii) to the measurement of a higher number of Bragg peaks and (iii) to increase the irradiated volume of the specimen. Figs. 3.10.1(*a*) and 3.10.1(*b*) show the irradiated volumes bathed by X-rays when using flat samples for Mo and Cu radiations in transmission geometry, and Fig. 3.10.1(*c*) shows the irradiated volume for Cu in reflection mode (Cuesta *et al.*, 2015). Mo radiation combined with a flat sample in transmission geometry allows an irradiated volume of close to 100 mm^3; meanwhile, for Cu radiation (flat samples in reflection and transmission geometries) the irradiated volumes are close to 5 mm^3 (Cuesta *et al.*, 2015). In this context, it is worth mentioning that the absorption correction for flat-

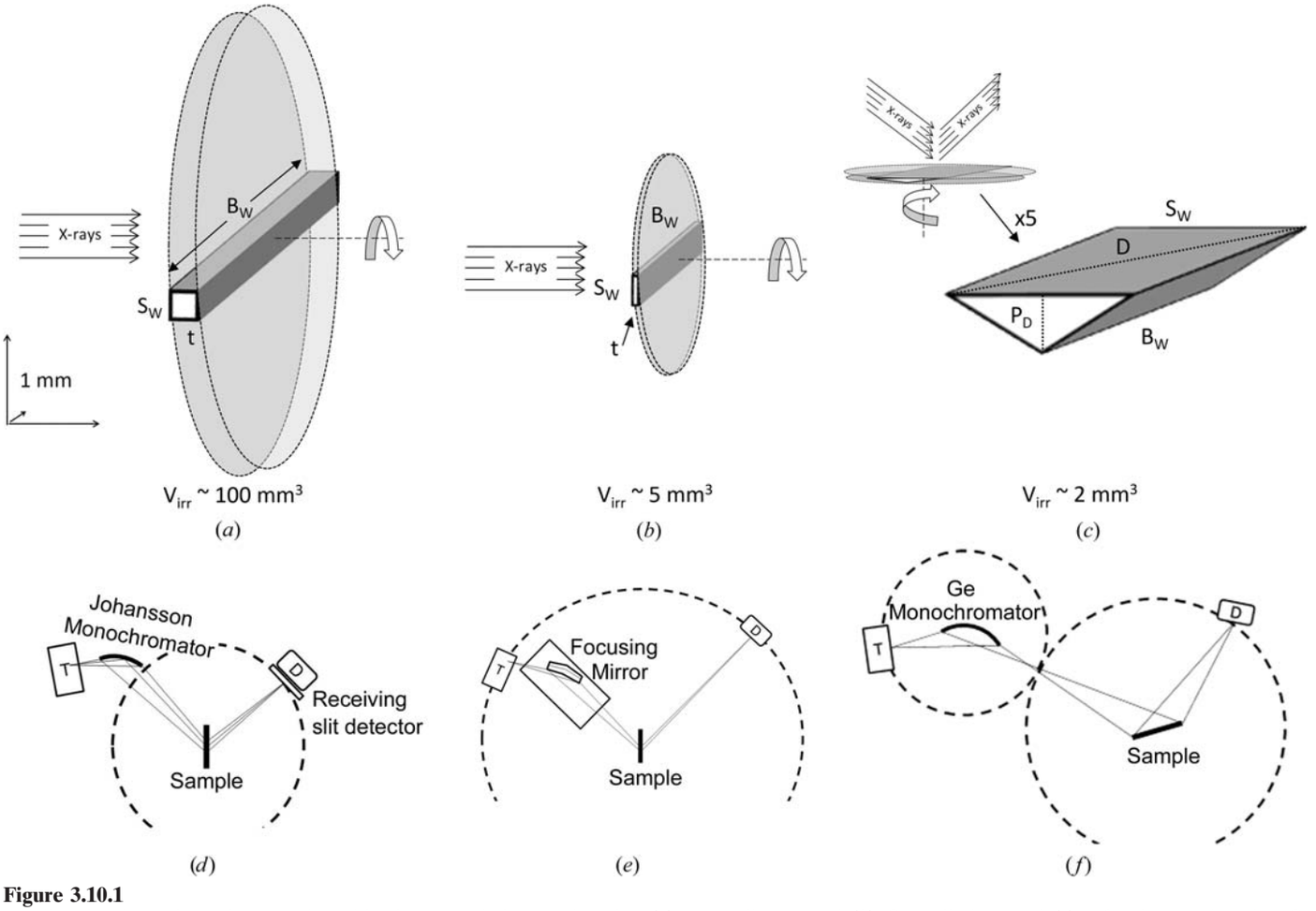

Figure 3.10.1
Irradiated volume for a flat sample holder in transmission mode using (*a*) Mo radiation and (*b*) Cu radiation, and (*c*) reflection mode using Cu radiation. Diffraction-geometry sketches: (*d*) transmission geometry with primary monochromator, (*e*) transmission geometry with focusing mirror and (*f*) reflection geometry with primary monochromator. [Reprinted from Cuesta *et al.* (2015) with permission from Cambridge University Press.]

Table 3.10.1
Cambridge Structural Database (CSD)/Inorganic Crystal Structure Database (ICSD) reference codes for all phases used for Rietveld refinements in this work and the linear absorption coefficients for the wavelengths used

Phase	Chemical formula	CSD/ICSD refcode	μ (cm^{-1}), Cu $K\alpha_1$, λ = 1.5406 Å	μ (cm^{-1}), Mo $K\alpha_1$, λ = 0.7093 Å	μ (cm^{-1}), λ = 0.7744/0.4959 Å	Reference
Glucose	$C_6H_{12}O_6$	Glucsa10	12	1	1.3/—	Brown & Levy (1979)
Fructose	$C_6H_{12}O_6$	Fructo11	12	1	1.3/—	Kanters *et al.* (1977)
α-Lactose monohydrate	$C_{12}H_{22}O_{11}{\cdot}H_2O$	Lactos10	12	1	1.3/—	Fries *et al.* (1971)
Xylose	$C_5H_{10}O_5$	Xylose	12	1	1.2/—	Hordvik (1971)
Gypsum	$CaSO_4{\cdot}(H_2O)_2$	151692	141	16	22/—	De la Torre *et al.* (2004)
Quartz	SiO_2	41414	92	10	11/2.9	Will *et al.* (1988)
s-Anhydrite	$CaSO_4$	16382	219	24	31/—	Kirfel & Will (1980)
i-Anhydrite	$CaSO_4$	79527	219	24	31/—	Bezou *et al.* (1995)
Zincite	ZnO	65120	285	244	—/89.1	Albertsson *et al.* (1989)
Calcite	$CaCO_3$	80869	194	22	27/7.3	Maslen *et al.* (1995)
$SrSO_4$	$SrSO_4$	22322	299	187	40/—	Garske & Peacor (1965)

sample transmission geometry is conceptually similar to that for flat-plate reflection geometry, but the length of the scattered beam path has to be properly defined. The corresponding equation is given in section A5.2.5 of Egami & Billinge (2003).

It must also be noted that Mo radiation has a major drawback when compared with Cu radiation. The λ^3 dependence of diffraction intensity favours the use of Cu radiation by a factor of 10.2. Thus, a detector receives approximately ten times as many diffracted X-ray photons with Cu than with Mo (this calculation neglects the different fractions of photons lost in the diffractometer optical paths). This fact can be partially overcome in modern X-ray detectors by increasing the counting time for patterns collected with Mo radiation without reaching prohibitively long times.

As discussed in Chapter 3.9, there are many factors that affect the accuracy and precision of QPA results. It must be recalled that accuracy is the agreement between the analytical result and the true value, and precision is the agreement between results for analyses repeated under the same conditions. Precision may be further divided into repeatability, the agreement between analyses derived from several measurements on the same specimen, and reproducibility, the agreement including re-preparation, re-measurement and data re-analysis of the same sample. Since the largest sources of errors in RQPA are experimental, sample preparation is key, as the reproducibility of peak-intensity measurements is mainly governed by particle statistics (Elton & Salt, 1996). It is generally accepted that the diffraction intensities have to be collected with an accuracy close to $\pm 1\%$ to obtain patterns that are suitable for good RQPA procedures (Von Dreele & Rodriguez-Carvajal, 2008). Milling the sample to reduce the particle size is an approach that should be exercised with care to avoid peak broadening or amorphization (Buhrke *et al.*, 1998). In order to improve particle statistics, a very common practice is to continuously spin the sample during data collection. A much less developed approach is to use high-energy, highly penetrating laboratory X-rays.

Another important issue in the QPA of mixtures is the limit of detection (LoD) and the limit of quantification (LoQ). In this context, the LoD can be defined as the minimal concentration of analyte that can be detected with acceptable reliability (Zevin & Kimmel, 1995), *i.e.* for which its strongest (not overlapped) diffraction peak in the powder pattern has a signal-to-noise ratio larger than 3.0. The 'reliability' criterion is flexible and may be defined by regulatory agencies, as is mainly the case for active pharmaceutical ingredients. Evidently, the LoD can be reduced (improved) by increasing the intensity of the X-ray source, for example using synchrotron radiation. In this context, the LoQ can be defined as the minimum content of an analyte that can be determined with a value at least three times larger than its standard deviation and determined to an acceptable reliability level. For RQPA, this type of approach can be straightforward, although the accuracy for minor phases may be quite poor.

The main aim of the study described here was to test whether the use of high-energy Mo radiation, combined with high-resolution X-ray optics, could yield more accurate RQPA than well established procedures using Cu radiation. In order to do so, three sets of mixtures with increasing amounts of a given phase (the spiking method) were prepared and the corresponding RQPA results were evaluated with calibration curves (least-squares fits) and quantitatively by statistical analysis based on the Kullback–Leibler distance (KLD; Kullback, 1968). The three series were (i) crystalline inorganic phase mixtures with increasing amounts of an inorganic phase, (ii) crystalline organic phase mixtures with increasing amounts of an organic compound and (iii) a series with an increasing content of amorphous ground glass. This last series is the most challenging case because the amorphous content is derived from a small overestimation of the internal standard employed. Amorphous content determination is important for many industries, including cements, glasses, pharmaceuticals and alloys.

3.10.2. Compounds and series

3.10.2.1. *Single phases*

Table 3.10.1 provides information about the phases used in this work. Further details can be found in the original publication (León-Reina *et al.*, 2016). All of the mixtures were prepared by grinding the weighed phases by hand in an agate pestle and mortar for 20 min to ensure homogeneity.

3.10.2.2. *Crystalline inorganic series*

A constant matrix of calcite (C), gypsum (Gp) and quartz (Q) was prepared. Six samples with known increasing amounts of insoluble anhydrite (i-A) were then produced and were labelled CGpQ_*x*A, where *x* repesents the target i-A content: 0.00, 0.125, 0.25, 0.50, 1.0, 2.0 or 4.0 wt%.

3.10.2.3. *Crystalline organic series*

A constant matrix of glucose (G), fructose (F) and lactose (L) was prepared. Six samples with known increasing amounts of xylose (X) were then produced and labelled GFL_*x*X, where *x* represents the target X content: 0.00, 0.125, 0.25, 0.50, 1.0, 2.0 or 4.0 wt%.

3.10.2.4. *Variable amorphous content series*

A constant matrix of calcite (C) and zincite (Z) was prepared. Five samples with increasing contents of amorphous ground glass (Gl) were then prepared. The elemental composition of the ground glass is given in García-Maté *et al.* (2014). The mixtures were labelled CZQ_*x*Gl, where *x* indicates 0, 2, 4, 8, 16 or 32 wt% Gl. The amorphous content was determined by adding ∼20 wt% quartz (Q) as an internal standard.

3.10.3. Analytical techniques

All phases and mixtures were studied with Mo $K\alpha_1$ (transmission geometry) and Cu $K\alpha_1$ (reflection geometry) monochromatic radiation. Table 3.10.1 shows the X-ray linear absorption coefficients for all of the phases, as microabsorption is always a concern in RQPA. A microabsorption correction was not applied in this work, but readers must be aware that this effect, if relevant, is one of the greatest source of inaccuracy in RQPA (Madsen *et al.*, 2001; Scarlett *et al.*, 2002). All of the phases were also characterized by scanning electron microscopy (see Fig. 3.10.2).

3.10.3.1. *Mo $K\alpha_1$ laboratory X-ray powder diffraction (LXRPD)*

Mo $K\alpha_1$ powder patterns were collected in transmission geometry in constant irradiated volume mode, in order to avoid any correction of the measured intensities, on a D8 ADVANCE (Bruker AXS) diffractometer (188.5 mm radius) equipped with a Ge(111) primary monochromator, which gives monochromatic Mo radiation (λ = 0.7093 Å). The X-ray tube operated at 50 kV and 50 mA. The optics configuration was a fixed divergence slit (2°) and a fixed diffracted anti-scatter slit (9°). A LYNXEYE XE 500 µm energy-dispersive linear detector, optimized for high-energy radiation, was used with the maximum opening angle. Using these conditions, the samples were measured between 3 and 35° 2θ with a step size of 0.006° and with a total measurement time of 3 h 5 min. The flat samples were placed into cylindrical holders between two Kapton foils (Cuesta *et al.*, 2015) and rotated at a rate of 10 revolutions per minute during data collection. Moreover, the absorption factor of each sample was experimentally measured by comparing the direct beam with and without the sample (Cuesta *et al.*, 2015). The amount of sample loaded (which determines the height of the cylinder) in the holders was adjusted to obtain a total absorption (μt) of ∼1, which corresponds to an absorption factor of ∼2.7 or 63% of direct-beam attenuation. For the organic samples this criterion was not followed as it would lead to very thick specimens. In this case, the maximum holder thickness was used (1.7 mm).

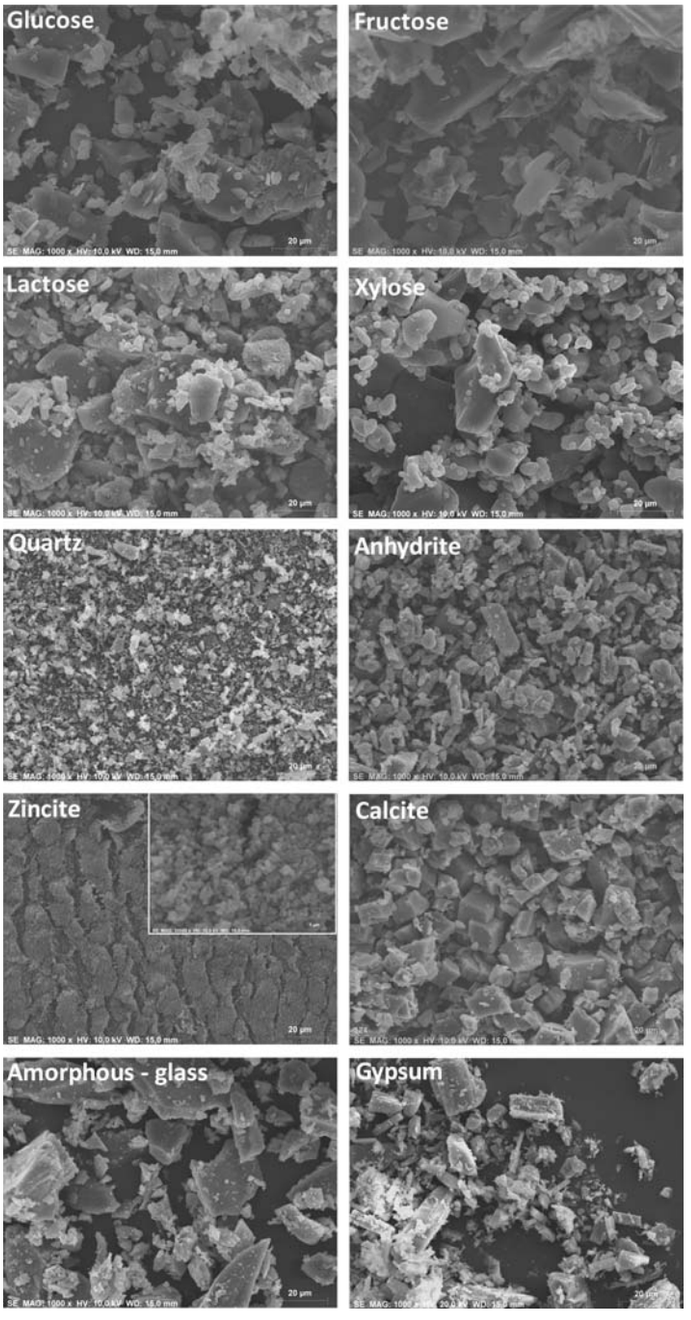

Figure 3.10.2
Scanning electron microscopy micrographs for the studied phases (×1000). The inset in the zincite micrograph shows the powder at higher magnification (×20 000).

3.10.3.2. *Cu $K\alpha_1$ laboratory X-ray powder diffraction (LXRPD)*

Cu $K\alpha_1$ powder patterns for exactly the same samples were recorded in reflection geometry ($\theta/2\theta$) on a X′Pert MPD PRO (PANalytical B.V.) diffractometer (240 mm radius) equipped with a Ge(111) primary monochromator, which gives monochromatic Cu radiation (λ = 1.54059 Å). The X-ray tube was operated at 45 kV and 40 mA. The optics configuration was a fixed divergence slit (0.5°), a fixed incident anti-scatter slit (1°), a fixed diffracted anti-scatter slit (0.5°) and an X′Celerator RTMS (real-time multiple strip) detector operating in scanning mode with the maximum active length. Using these conditions, the samples were measured between 6.5 and 81.5° 2θ with a step size of 0.0167° and a total measurement time of 2 h 36 min. The flat samples were prepared by rear charge of a flat sample holder in order to minimize preferred orientation and were rotated at a rate of 10 revolutions per minute.

The lowest analyte content samples, CGpQ_0.12A and GFL_0.12X, were measured three times using both radiations, Mo $K\alpha_1$ and Cu $K\alpha_1$, for a precision (reproducibility) assessment. Therefore, regrinding and reloading of the mixtures in the sample holder was carried out prior to every measurement.

3.10.3.3. *Transmission synchrotron X-ray powder diffraction (SXRPD)*

Powder patterns for the lowest analyte content samples, CGpQ_0.12A and GFL_0.12X, were also measured using synchrotron radiation. SXRPD data were collected in Debye–Scherrer (transmission) mode using the powder diffractometer at

the ALBA Light Source (Fauth *et al.*, 2013). The wavelength, λ = 0.77439 (2) Å, was selected with a double-crystal Si(111) monochromator and was determined using the NIST SRM640d Si standard (a = 5.43123 Å). The diffractometer is equipped with a MYTHEN-II detector system. The samples were loaded into glass capillaries 0.7 mm in diameter and were rapidly rotated during data collection to improve the diffracting-particle statistics. The data-acquisition time was 20 min per pattern to attain a very good signal-to-noise (S/N) ratio over the angular range 1–35° 2θ. Three patterns, taken at different positions along the capillaries, were collected for each sample.

SXRPD data for the amorphous content series, CZQ_xGl, were also measured at the ALBA Light Source. The experimental setup was the same as described above but the working wavelength was λ = 0.49591 (2) Å.

3.10.4. Powder-diffraction data analysis

All powder patterns were analysed by the Rietveld method using the *GSAS* software package (Larson & Von Dreele, 2000) with the pseudo-Voigt peak-shape function (Thompson *et al.*, 1987) for RQPA. The refined overall parameters were phase scale factors, background coefficients (linear interpolation function), unit-cell parameters, zero-shift error, peak-shape parameters and preferred-orientation coefficient, when needed. The March–Dollase preferred-orientation adjustment algorithm was employed (Dollase, 1986). The modelling direction must be given as input for the calculations. In this case, the directions for the different phases were taken from previous studies. Alternatively, this direction can be extracted from the pattern from an analysis of the differences between observed and calculated intensities for non-overlapped diffraction peaks. The crystal structures used are reported in Table 3.10.1.

In order to provide a single numerical assessment of the performance of each analysis, a statistic based on the KLD distance was used (Kullback, 1968). This approach was previously used to evaluate the accuracy of RQPA applied to standard mixtures (Madsen *et al.*, 2001; Scarlett *et al.*, 2002; León-Reina *et al.*, 2009). Both phase-related KLD distances and absolute values of the Kullback–Leibler distance (AKLD) were calculated. Accurate analyses are mirrored by low values of AKLD.

The overall amorphous content was determined from the internal standard methodology approach (De la Torre *et al.*, 2001; Aranda *et al.*, 2012) with quartz as an internal standard [using isotropic atomic displacement parameters (ADPs) of 0.045 and 0.0087 Å^2 for Si and O, respectively]. If the original sample contains an amorphous phase, the amount of standard will be overestimated in RQPA. From the (slight) overestimation of the standard, the amorphous content of the investigated sample can be derived (De la Torre *et al.*, 2001). The important role of the values of the ADPs in the results of RQPA mainly in amorphous content determinations using the internal-standard method has been discussed previously (Madsen *et al.*, 2011).

3.10.5. Crystalline single phases

All of the single phases were selected according to several parameters, such as relevance to selected applications, purity, particle size of the powder and preferred orientation. In order to check the suitability of the crystal structures used, all of the phases were first studied using powder diffraction with Mo $K\alpha_1$ radiation. These preliminary studies were of special interest for organic phases, as the CIF files obtained from the Cambridge Structural Database (CSD) did not contain the atomic displacement parameters (ADPs). For lactose and fructose, the ADPs were obtained from the original publications and were introduced manually into the *GSAS* control file. For glucose and

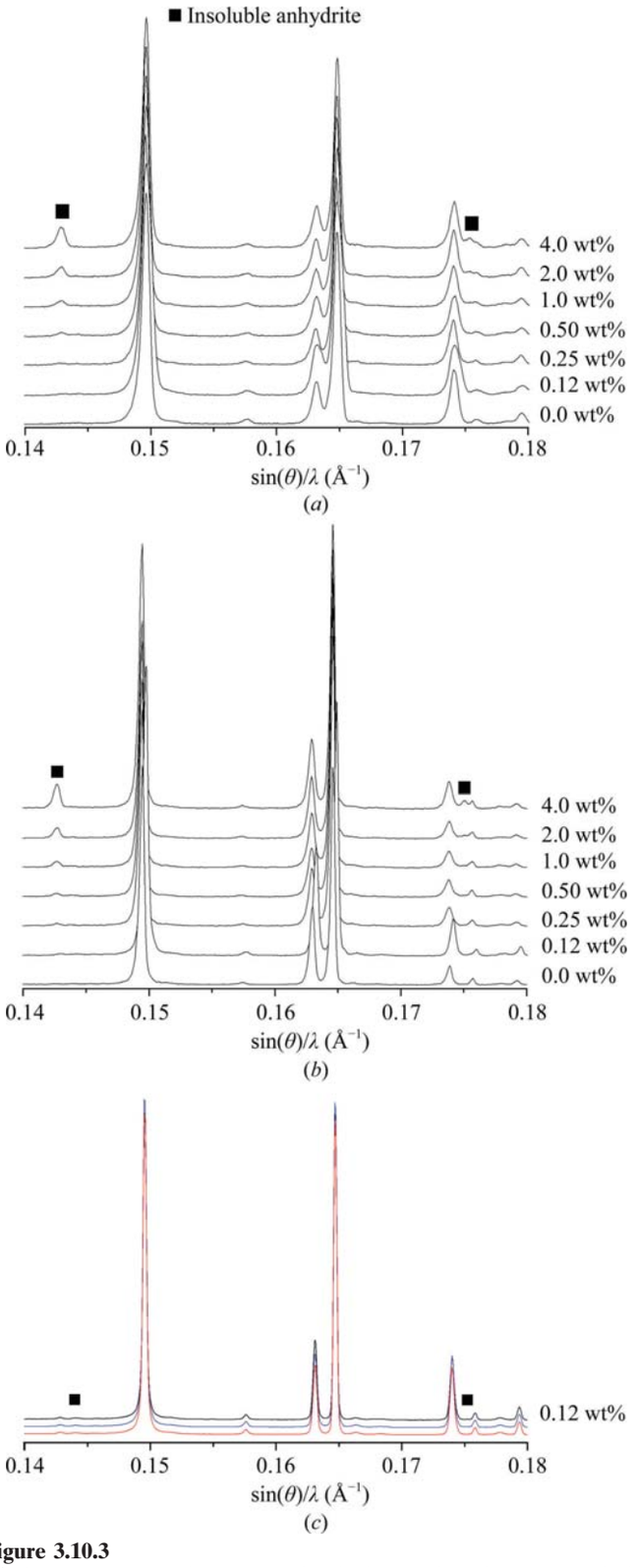

Figure 3.10.3
(*a*) Raw Mo $K\alpha_1$ powder patterns for the inorganic series composed of a constant matrix of calcite, gypsum and quartz, and increasing amounts of insoluble anhydrite (peaks highlighted with a solid square). (*b*) Raw Cu $K\alpha_1$ powder patterns for the same inorganic series. (*c*) Raw SXRPD patterns for CGpQ_0.12A collected at three different positions of the capillary (red, black and blue traces). The intensity values in (*c*) have been artificially offset to show the three different patterns.

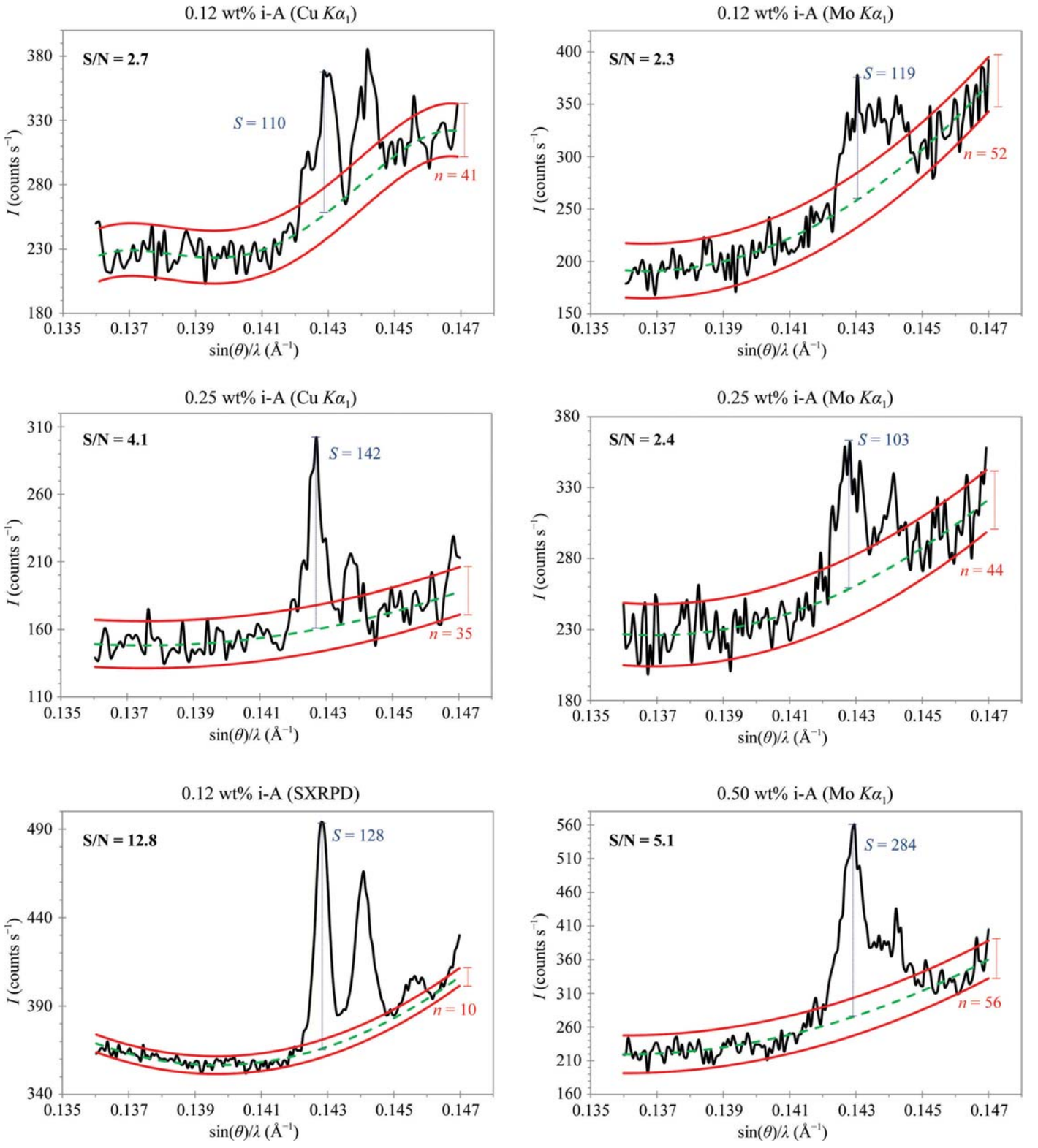

Figure 3.10.4
Selected region of the powder patterns showing the main diffraction peak of insoluble anhydrite for the low-content samples to investigate the limit of detection. Top left: Cu $K\alpha_1$ pattern for CGpQ_0.12A. Middle left, Cu $K\alpha_1$ pattern for CGpQ_0.25A. Bottom left, SXRPD pattern for CGpQ_0.12A. Top right, Mo $K\alpha_1$ pattern for CGpQ_0.12A. Middle right, Mo $K\alpha_1$ pattern for CGpQ_0.25A. Bottom right, Mo $K\alpha_1$ pattern for CGpQ_0.50A. The main peak of anhydrite, $(\theta)/\lambda = 0.143$ Å^{-1}, is located at 25.4, 11.6 and 12.7° 2θ for Cu $K\alpha_1$, Mo $K\alpha_1$ and synchrotron radiations, respectively. The peak at $\sin(\theta)/\lambda = 0.1445$ Å^{-1} is due to the soluble anhydrite from gypsum (constant content in all the samples). The very tiny peak at $\sin(\theta)/\lambda = 0.1457$ Å^{-1}, which is slightly visible only in the SXRPD pattern, arises from $SrSO_4$ (0.39 wt%) from gypsum.

xylose, the ADP values were not reported in the original publications. Hence, they were obtained from the fits to the Mo $K\alpha_1$ patterns for the single phases. Three groups of isotropic ADPs were refined: those for O, C and H atoms. The final ADP values are given in León-Reina *et al.* (2016) as well as the R_F values before and after optimization, showing the improvements in the fits. For RQPA of all of the mixtures the ADPs were kept fixed.

Preferred orientation was modelled by the March–Dollase algorithm along the [001] axis for both glucose and lactose. Since microparticle sizes and distributions for different phases may

result in some sample-related effects, such as preferred orientation, microabsorption and 'rock-in-the-dust/graininess' effects, all powders were characterized by scanning electron microscopy (SEM). Fig. 3.10.2 shows SEM micrographs for all of the phases. All inorganic samples were single phases except for gypsum and insoluble anhydrite. The impurity-phase contents for these two samples were reported in León-Reina *et al.* (2016).

Both organic and inorganic phases were also measured using Cu $K\alpha_1$ radiation in reflection mode. As expected, a transparency effect was observed in the Cu $K\alpha_1$ patterns for organic samples (Buhrke *et al.*, 1998).

3.10.6. Limits of detection and quantification

LoD and LoQ are two important quantities in the validation of any analytical method. LoD/LoQ are terms that are used to describe the smallest concentration of an analyte that can be reliably detected/assessed by an analytical procedure, as discussed in Section 3.10.1. In techniques such as Rietveld analysis, the approach of having a powder pattern with its strongest (not overlapped) diffraction peak with an S/N ratio of larger than 3.0 is not straightforward because the full powder pattern is evaluated.

Fig. 3.10.3 shows Mo $K\alpha_1$ and Cu $K\alpha_1$ raw patterns for the inorganic series with increasing amounts of insoluble anhydrite (labelled with solid squares) and Fig. 3.10.4 shows the strongest diffraction peak for i-A in the mixtures containing 0.123 wt% anhydrite (CGpQ_0.12A) and 0.25 wt% anhydrite (CGpQ_0.25A) to evaluate the limits of detection in the conditions reported in Section 3.10.5. For CGpQ_0.12A, both laboratory powder patterns yielded peaks with S/N ratios lower than 3.0 (top panels in Fig. 3.10.4). For CGpQ_0.25A, the Cu $K\alpha_1$ pattern yielded a clear peak with S/N = 4.1; therefore, it can be concluded that the LoD for insoluble anhydrite with this radiation in this mixture is slightly lower than 0.2 wt%. For Mo $K\alpha_1$ radiation, the CGpQ_0.25A and CGpQ_0.50A samples yielded patterns with peaks with S/N ratios of 2.4 and 5.1, respectively. Hence, it can be concluded that the LoD for i-A with this radiation in this mixture is quite close to 0.3 wt%.

The LoQ for i-A in this matrix was also studied. Three Mo $K\alpha_1$ and Cu $K\alpha_1$ patterns were collected for CGpQ_0.12A. For the three Mo $K\alpha_1$ patterns, the average analysis result for i-A was 0.28 (2) wt%, but the accuracy of the obtained value is poor, as the expected value was 0.12 wt%. Similarly, the average value for the analyses of three Cu $K\alpha_1$ patterns was 0.24 (2) wt%. The RQPA results are given as supporting information in León-Reina *et al.* (2016). It was concluded that i-A can be quantified in this mixture at the level of 0.12 wt%, but with a relative error close to 100%. If the 'acceptable reliability' criterion in the analysis is taken into consideration, the LoQ value would be close to 1.0 wt% in order to have a relative associated error lower than 20%.

CGpQ_0.12A was also studied by SXRPD. Fig. 3.10.3(*c*) shows the SXRPD patterns collected at three different positions of the capillary, which were almost identical, and Fig. 3.10.4 (bottom left) shows the main diffraction peak of anhydrite. The S/N ratio for the strongest diffraction peak of anhydrite was 12.8 and hence the limit of detection for i-A with synchrotron radiation in this matrix is below 0.10 wt%.

To quantify the accuracy of the analyses, the KLD methodology was used. The AKLD values for each analysis as well as the KLD values for i-A are reported in León-Reina *et al.* (2016). The synchrotron analyses clearly had better accuracy than those using laboratory radiation. Moreover, the Mo $K\alpha_1$ radiation analyses were slightly better than those obtained using Cu $K\alpha_1$ radiation.

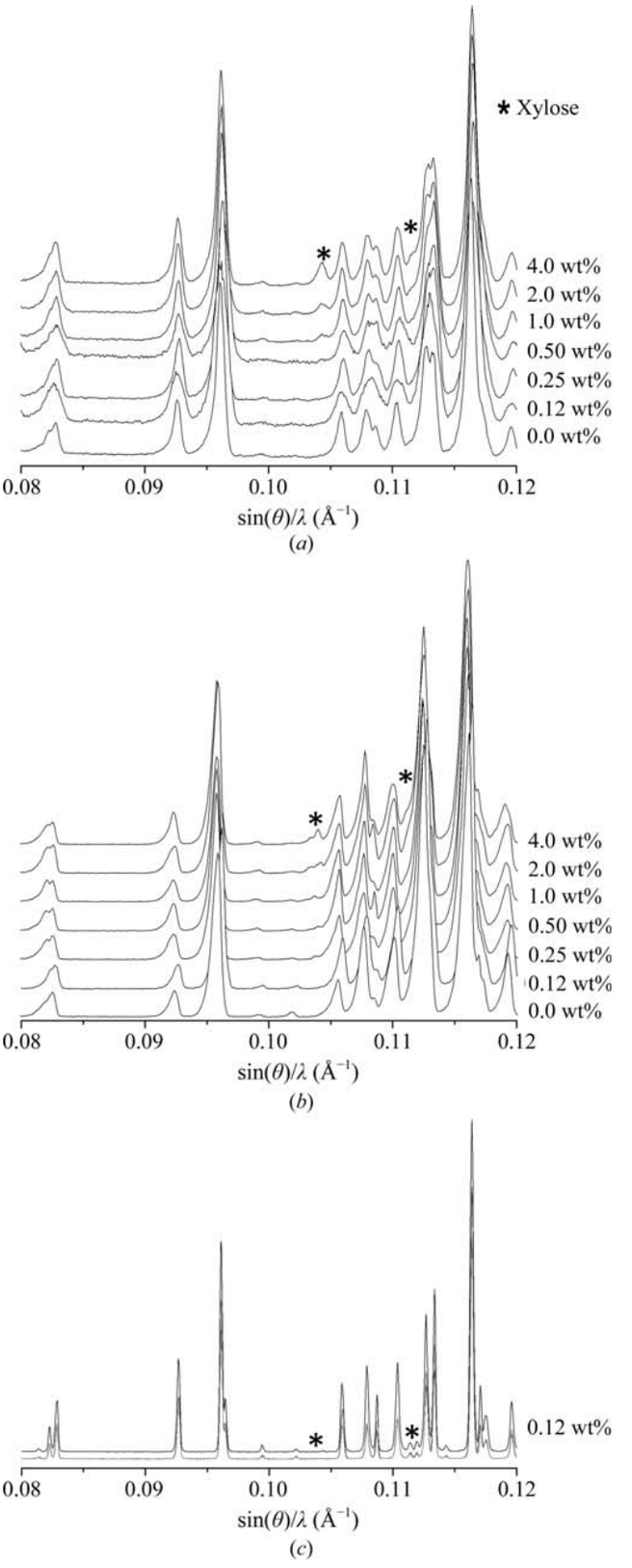

Figure 3.10.5
(*a*) Raw Mo $K\alpha_1$ powder patterns for the organic series composed of a constant matrix of glucose, fructose and lactose, and increasing amounts of xylose (peaks highlighted with an asterisk). (*b*) Raw Cu $K\alpha_1$ powder patterns for the same organic series. (*c*) Raw SXRPD patterns for GFL_0.12X collected at three different positions of the capillary (as collected).

Table 3.10.2
Rietveld quantitative phase analyses for the crystalline inorganic mixtures measured with Cu $K\alpha_1$ and Mo $K\alpha_1$ radiations

Weighed amounts (wt%) are also shown for comparison. Absolute values of the Kullback–Liebler distance (AKLD) for each mixture and the KLD value for i-anhydrite are also included. Trm, transmission; rfl, reflection.

	CGpQ_0.0A			CGpQ_0.25A			CGpQ_0.50A		
Phases	wt%	Mo trm	Cu rfl	wt%	Mo trm	Cu rfl	wt%	Mo trm	Cu rfl
C	32.9	32.6 (1)	30.4 (2)	32.8	32.0 (1)	33.6 (1)	32.7	33.2 (1)	32.8 (1)
Gp	31.7	31.7 (1)	34.5 (1)	31.7	32.5 (1)	31.6 (1)	31.6	30.1 (1)	30.7 (1)
Q	34.2	34.6 (1)	33.7 (1)	34.1	33.9 (1)	33.0 (1)	34.0	34.6 (1)	34.2 (1)
s-A	0.8	0.66 (3)	0.76 (5)	0.8	0.77 (4)	0.78 (5)	0.8	0.97 (3)	1.15 (5)
$SrSO_4$	0.4	0.44 (4)	0.70 (6)	0.4	0.44 (4)	0.67 (5)	0.4	0.39 (4)	0.56 (5)
i-A	—	—	—	0.28	0.42 (3)	0.42 (4)	0.52	0.71 (3)	0.71 (4)
AKLD sum		0.0089	0.0605		0.0198	0.0235		0.0295	0.0180
(i-A) KLD					−0.001	−0.001		−0.002	−0.002

	CGpQ_1.0A			CGpQ_2.0A			CGpQ_4.0A		
Phases	wt%	Mo trm	Cu rfl	wt%	Mo trm	Cu rfl	wt%	Mo trm	Cu rfl
C	32.5	32.8 (1)	32.6 (2)	32.2	31.3 (1)	31.4 (1)	31.6	31.2 (1)	31.8 (1)
Gp	31.5	30.4 (1)	30.7 (1)	31.1	32.1 (1)	32.3 (1)	30.5	30.7 (1)	30.5 (1)
Q	33.8	34.1 (1)	33.8 (1)	33.5	33.5 (1)	32.6 (1)	32.8	32.8 (1)	32.0 (1)
s-A	0.8	1.03 (4)	1.11 (5)	0.7	0.54 (3)	0.58 (5)	0.7	0.67 (3)	0.77 (4)
$SrSO_4$	0.4	0.43 (4)	0.68 (5)	0.4	0.48 (4)	0.68 (6)	0.4	0.45 (4)	0.63 (5)
i-A	1.02	1.23 (3)	1.17 (5)	2.02	2.05 (4)	2.38 (9)	4.02	4.30 (8)	4.33 (9)
AKLD sum		0.0214	0.0152		0.0218	0.0358		0.0095	0.0156
(i-A) KLD		−0.002	−0.001		0.000	−0.003		−0.004	−0.003

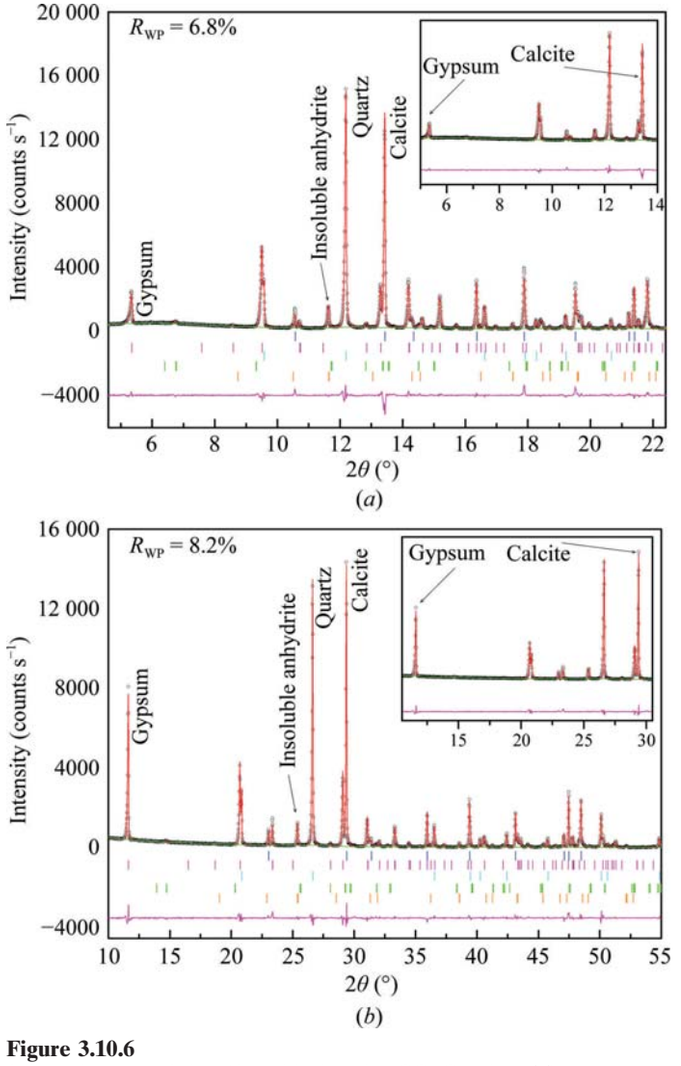

Figure 3.10.6
Selected range of the Rietveld plots for CGpQ_4.0A: (*a*) Mo $K\alpha_1$ and (*b*) Cu $K\alpha_1$ patterns. The inset highlights the effect of preferred orientation for gypsum and calcite.

Fig. 3.10.5 shows Mo $K\alpha_1$ and Cu $K\alpha_1$ raw patterns of the organic mixtures with increasing amounts of xylose. The strongest powder-diffraction peak for xylose in the GFL_0.12X patterns (with both Mo and Cu radiations) was not observed. The corresponding peak was observed in the GFL_0.25X patterns. Therefore, the LoD can be established as close to 0.25 wt%. The analysis results for xylose in GFL_0.25X were reported in León-Reina *et al.* (2016). These values showed that the results from Mo $K\alpha_1$ powder diffraction were slightly more accurate.

The LoQ for xylose was also studied. Once again, three Mo $K\alpha_1$ and Cu $K\alpha_1$ patterns were collected for GFL_0.12X. The average value for the analysis of the three Mo patterns was 0.18 (8) wt%. Similarly, the average result for the analyses of three Cu patterns was 0.34 (6) wt%. Full RQPA results are reported in the supporting information of León-Reina *et al.* (2016). The LoQ for xylose in this mixture for the two radiations can be established as close to 0.12 wt%. Indeed, if one applies an 'acceptable reliability' criterion, the LoQ would be much higher at above 1 wt%. The output of this study was that Cu $K\alpha_1$ radiation yielded a slightly less accurate result than that obtained from the Mo $K\alpha_1$ data.

GFL_0.12X was also studied by SXRPD in a rotating glass capillary in transmission mode. Fig. 3.10.5(*c*) shows SXRPD patterns for GFL_0.12X collected at three different positions of the same capillary. The powder patterns showed quite different peak ratios. It is important to bear in mind that filling a glass capillary with organic compounds is sometimes not easy due to electrostatic charge effects. For this reason, the phase ratio within the part of capillary bathed by the X-rays might not be the same as that of the sample under study. The behaviour observed in Fig. 3.10.5(*c*) could be explained by inhomogeneous capillary filling. Hence, in this case, the RQPA results are unreliable. Even in 'well behaved' samples, inhomogeneous filling of small capillaries could result in problems. Readers should be aware of this, and the authors strongly recommend that at least three patterns should be collected along the capillary and superimposed. If there is inhomogeneous filling the patterns will differ, and extreme care

has to be exercised when filling capillaries in order to minimize this problem.

3.10.7. Increasing inorganic crystalline phase content series

Table 3.10.2 reports the RQPA results for six inorganic mixtures with increasing amounts of i-A measured with Mo $K\alpha_1$ (transmission) and Cu $K\alpha_1$ (reflection). The Rietveld plots of the mixture with 4 wt% i-A are shown in Fig. 3.10.6. For most of the samples, the AKLD values (see Table 3.10.2) for Mo $K\alpha_1$ radiation are slightly smaller than the corresponding values obtained for Cu $K\alpha_1$ radiation. For this reason, we can conclude that the Mo $K\alpha_1$ analyses are slightly better than those derived using Cu $K\alpha_1$ radiation.

On the other hand, calcite and gypsum presented preferred orientations, with the axes being [104] and [010], respectively. This effect was modelled using the March–Dollase algorithm. Preferred orientation makes the $0l0$ reflections for gypsum have higher intensities in the Cu $K\alpha_1$ patterns, and smaller intensities in the Mo $K\alpha_1$ patterns, than those calculated from the crystal structure (see insets in Fig. 3.10.6). As a consequence, the refined values for flat samples in reflection and transmission geometries were smaller and larger than 1.0, respectively (Cuesta *et al.*, 2015). Although preferred orientation is present in all patterns, the Cu $K\alpha_1$ patterns were recorded in reflection geometry (flat samples), while the Mo $K\alpha_1$ measurements were collected in transmission (also flat samples). This results in opposite diffraction intensity changes and points towards another (possible) fruitful use: joint refinement of these two types of patterns to counterbalance the effects of preferred orientation in RQPA.

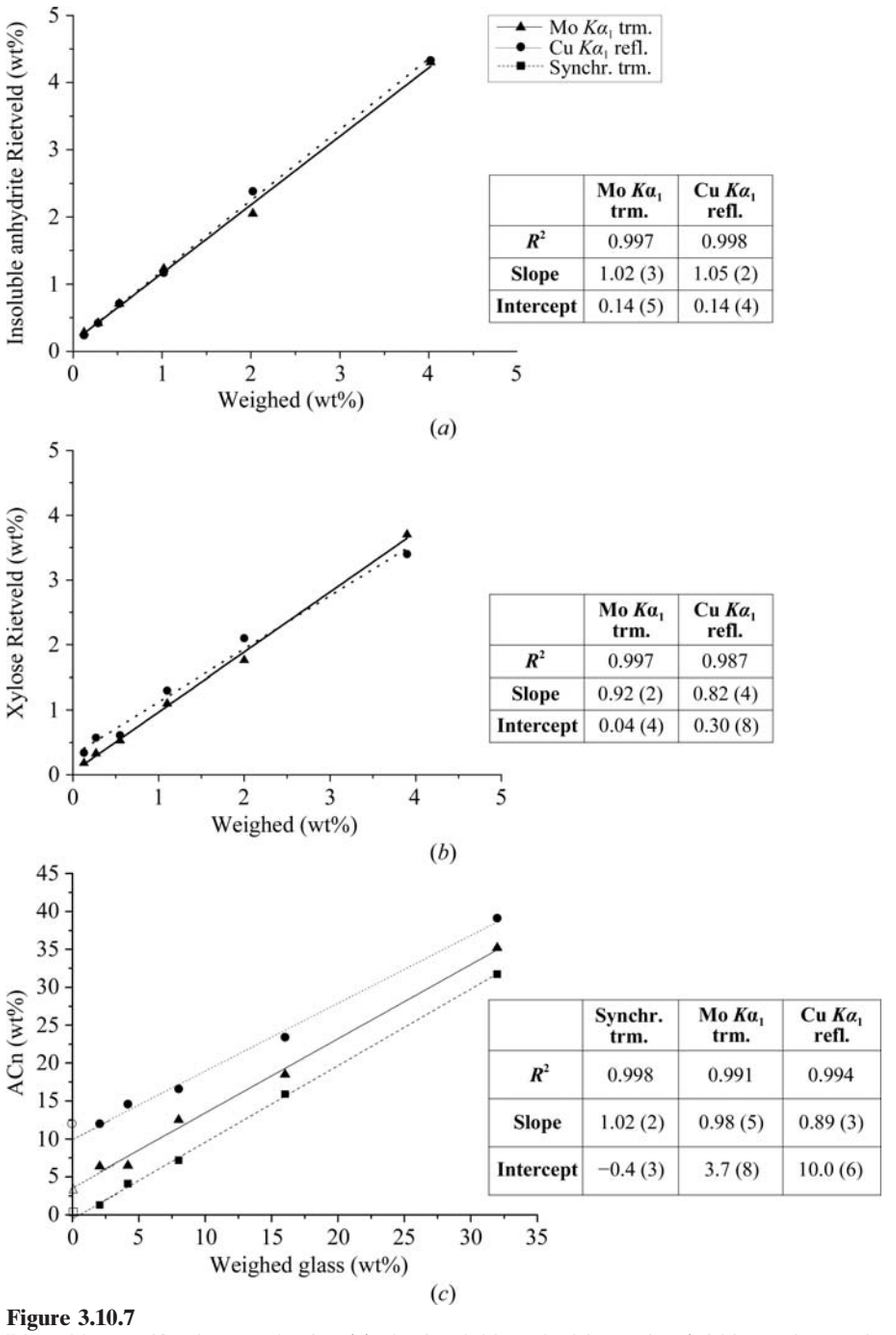

	Mo $K\alpha_1$ trm.	Cu $K\alpha_1$ refl.
R^2	0.997	0.998
Slope	1.02 (3)	1.05 (2)
Intercept	0.14 (5)	0.14 (4)

	Mo $K\alpha_1$ trm.	Cu $K\alpha_1$ refl.
R^2	0.997	0.987
Slope	0.92 (2)	0.82 (4)
Intercept	0.04 (4)	0.30 (8)

	Synchr. trm.	Mo $K\alpha_1$ trm.	Cu $K\alpha_1$ refl.
R^2	0.998	0.991	0.994
Slope	1.02 (2)	0.98 (5)	0.89 (3)
Intercept	−0.4 (3)	3.7 (8)	10.0 (6)

Figure 3.10.7
Rietveld quantification results for (*a*) the insoluble anhydrite series (within an inorganic crystalline matrix), (*b*) the xylose series (within an organic crystalline matrix) and (*c*) the ground-glass series (within an inorganic crystalline matrix) as a function of the weighed amount of each phase. Open symbols represent the derived amorphous contents in the mixtures without any added glass. The results of the least-squares fits are also shown.

Fig. 3.10.7(*a*) shows the quantified i-A contents (wt%), as determined by the Rietveld methodology, as a function of the weighed i-A amount. The two R^2 values for the fits are very close to 1.00, and the intercept values are very close to zero, showing the appropriateness of the Rietveld methodology for quantifying crystalline materials. Furthermore, the slopes of the calibration curves are also 1.00 in both cases. Consequently, this study allows it to be concluded that RQPA for crystalline inorganic phases using powder-diffraction patterns collected using Mo $K\alpha_1$ radiation yields results that are as accurate as those obtained from the well established method using Cu $K\alpha_1$.

3.10.8. Increasing crystalline organic phase content series

Table 3.10.3 shows RQPA results for six mixtures prepared with G, F, L and an increasing amount of X measured with Mo $K\alpha_1$ (transmission) and Cu $K\alpha_1$ (reflection). In general, the values obtained using both radiations are quite similar to the weighed values. The AKLD values and the KLD values for the xylose phase are also reported in Table 3.10.3. The AKLD values from Mo $K\alpha_1$ and Cu $K\alpha_1$ radiations are relatively similar. The main problem for RQPA of organic mixtures measured in reflection geometry is related to the low X-ray absorption of the samples and the transparency effects that lead to poor peak shapes and even some split peaks in the powder patterns, as discussed previously (León-Reina *et al.*, 2016).

Fig. 3.10.7(*b*) shows the quantified xylose contents (wt%) as determined by the Rietveld methodology as a function of the weighed amount of xylose added to the mixtures. The results were plotted to obtain the calibration lines with increasing content of the analyte. Both plots gave R^2 values close to 1.0. However, the slope values were 0.92 and 0.82 for Mo $K\alpha_1$ and Cu $K\alpha_1$ radiations, respec-

Table 3.10.3
RQPA for the crystalline organic mixtures measured with Cu $K\alpha_1$ and Mo $K\alpha_1$ radiations

Weighed amounts (wt%) are also shown for the sake of comparison. Absolute values of the Kullback–Liebler distance (AKLD) for each mixture and the KLD value for xylose are also included. Trm, transmission; rfl, reflection.

	GFL_0.0X			GFL_0.25X			GFL_0.50X		
Phases	wt%	Mo trm	Cu rfl	wt%	Mo trm	Cu rfl	wt%	Mo trm	Cu rfl
G	33.4	33.8 (1)	33.5 (3)	33.3	33.6 (1)	33.1 (2)	33.2	32.3 (2)	33.5 (2)
F	33.5	31.7 (1)	32.7 (3)	33.4	32.3 (1)	34.3 (2)	33.3	32.1 (2)	33.4 (2)
L	33.1	34.5 (1)	33.7 (3)	33.0	33.7 (1)	32.0 (2)	33.0	35.0 (3)	32.5 (2)
X	—	—		0.27	0.33 (4)	0.57 (9)	0.55	0.53 (8)	0.61 (9)
AKLD sum		0.0362	0.0150		0.0216	0.0231		0.0410	0.0096
(X) KLD		—	—		−0.001	−0.002		0.000	−0.001

	GFL_1.0X			GFL_2.0X			GFL_4.0X		
Phases	wt%	Mo trm	Cu rfl	wt%	Mo trm	Cu rfl	wt%	Mo trm	Cu rfl
G	33.0	34.7 (1)	33.6 (2)	32.7	32.2 (1)	31.5 (2)	32.0	32.8 (1)	33.6 (2)
F	33.1	32.6 (1)	33.7 (2)	32.8	31.7 (1)	34.4 (2)	32.2	30.7 (1)	32.5 (2)
L	32.8	31.6 (2)	31.4 (2)	32.5	34.3 (1)	32.0 (2)	31.8	32.9 (1)	30.5 (2)
X	1.1	1.10 (5)	1.3 (1)	2.0	1.76 (5)	2.1 (1)	3.9	3.70 (5)	3.4 (2)
AKLD sum		0.0338	0.0280		0.0363	0.0339		0.0361	0.0372
(X) KLD		0.000	−0.002		0.003	−0.001		0.002	0.005

Table 3.10.4
Rietveld quantitative phase analyses of the CQZ_*x*Gl mixture, where quartz (Q) is the internal standard, to derive amorphous content (am), obtained from SXRPD, Mo $K\alpha_1$ and Cu $K\alpha_1$ patterns

Absolute values of the Kullback–Liebler distance (AKLD) for each mixture and the KLD value for the amorphous content are also included. Trm, transmission; rfl, reflection.

	Weighed			Synchrotron trm				
Mixture	C wt%	Z wt%	Gl wt%	C wt%	Z wt%	Am wt%	AKLD sum	Am KLD
CZQ_0Gl	50.01	49.99	0.00	49.9 (1)	49.6 (1)	0.4 (1)	0.0050	—
CZQ_2Gl	48.98	48.96	2.05	49.7 (1)	49.0 (1)	1.3 (1)	0.0169	0.009
CZQ_4Gl	47.93	47.91	4.17	47.9 (1)	47.6 (1)	4.5 (1)	0.0066	−0.003
CZQ_8Gl	46.00	46.00	7.99	46.6 (1)	45.9 (1)	7.5 (1)	0.0120	0.005
CZQ_16Gl	41.99	41.99	16.01	42.0 (1)	41.6 (1)	16.4 (1)	0.0079	−0.004
CZQ_32Gl	34.00	34.00	31.99	34.0(1)	33.7 (1)	32.3 (1)	0.0061	−0.003

	Mo $K\alpha_1$ trm					Cu $K\alpha_1$ rfl				
Mixture	C wt%	Z wt%	Am wt%	AKLD sum	Am KLD	C wt%	Z wt%	Am wt%	AKLD sum	Am KLD
CZQ_0Gl	47.5 (1)	49.0 (1)	3.5 (1)	0.0358	—	47.2 (1)	40.8 (1)	12.0 (1)	0.1305	—
CZQ_2Gl	45.9 (1)	47.7 (1)	6.4 (1)	0.0679	−0.023	47.4 (1)	40.6 (1)	12.0 (1)	0.1440	−0.036
CZQ_4Gl	46.5 (1)	47.0 (1)	6.5 (1)	0.0422	−0.019	45.8 (1)	39.7 (1)	14.6 (1)	0.1641	−0.052
CZQ_8Gl	42.6 (1)	44.8 (1)	12.5 (1)	0.0832	−0.036	45.3 (1)	38.1 (1)	16.6 (1)	0.1522	−0.058
CZQ_16Gl	39.9 (1)	41.7 (1)	18.5 (1)	0.0475	−0.023	40.9 (1)	35.8 (1)	23.4 (1)	0.1388	−0.061
CZQ_32Gl	31.7 (1)	33.1 (1)	35.2 (1)	0.0635	−0.031	32.2 (1)	28.7 (1)	39.1 (1)	0.1403	−0.064

tively. Slope values close to 1.0 mirror accurate analyses. Furthermore, the *y*-intercept values were 0.04 and 0.30 for Mo $K\alpha_1$ and Cu $K\alpha_1$ radiations, respectively. A *y*-intercept value close to 0.0 mirrors accurate analyses. Hence, it can be concluded that slightly more accurate analyses are obtained for Mo $K\alpha_1$ powder diffraction in transmission when compared with Cu $K\alpha_1$ powder diffraction in reflection for organic crystalline samples.

3.10.9. Increasing amorphous content series within an inorganic crystalline phase matrix

Fig. 3.10.8 shows Mo $K\alpha_1$ (transmission), Cu $K\alpha_1$ (reflection) and SXRPD (transmission) raw patterns for the mixtures with increasing amounts of glass. It is important to highlight that the increase in the background due to the glass is very modest even for ∼32 wt% of glass. Table 3.10.4 shows the RQPA of these mixtures, prepared with C, Z and an increasing amount of Gl, for the three radiations. The glass-free sample may contain amorphous material from the employed phases. Hence, we used the SXRPD data to calculate a correction factor for quartz to yield zero amorphous content for the glass-free sample (León-Reina *et al.*, 2016).

The linear fit to the amorphous content values obtained using SXRPD was very good, R^2 = 0.998, with the slope being 1.00 within the errors (see Fig. 3.10.7*c*). This plot also shows the quantified amorphous contents, in weight percentage, as a function of the amount of added ground glass, measured with Mo $K\alpha_1$ and Cu $K\alpha_1$ radiations. Open symbols indicate the derived amorphous contents obtained with the internal-standard method in the mixture without any added glass, CZQ_0Gl. Both R^2 values are quite close to 1.00, showing the consistency of the internal-standard methodology. However, the slope values were 0.98 and 0.89 for Mo $K\alpha_1$ and Cu $K\alpha_1$ radiations, respectively. Furthermore, the *y*-intercept values were 3.7 and 10.0 for Mo $K\alpha_1$ and Cu $K\alpha_1$ radiations, respectively. Again, slope values close to 1.0 and *y* intercepts close to 0.0 mirror accurate analyses. It must also

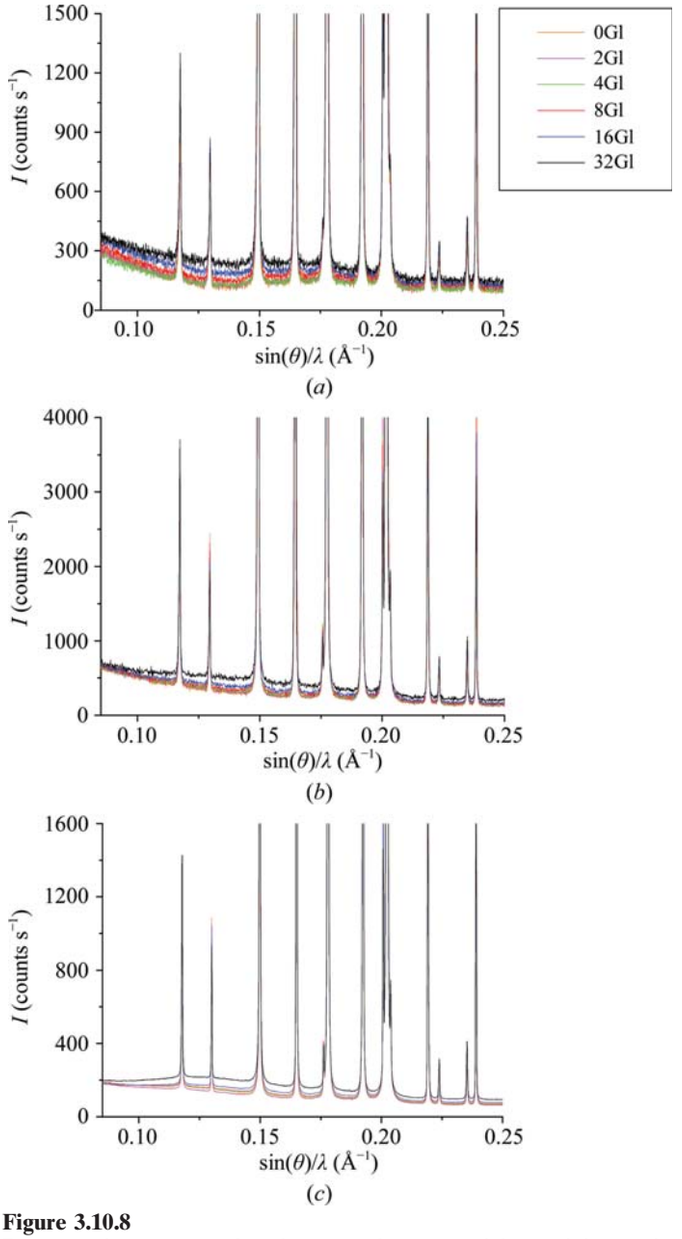

Figure 3.10.8
Raw powder patterns for the amorphous-material-containing series composed of a constant matrix of calcite and zincite, and increasing amounts of ground glass. Quartz was added as internal standard. (*a*) Mo $K\alpha_1$, (*b*) Cu $K\alpha_1$ and (*c*) SXRPD radiations. The intensities of the patterns have been rescaled to highlight the contributions of the glass to the background.

be pointed out that for the Mo $K\alpha_1$ analyses the value from the measurement of the Gl-free sample, 3.5 wt%, matches the value from the *y* intercept of the plot, 3.7 wt%, very well. Meanwhile, there is a much larger discrepancy for the similar Cu-based analyses, 12.0 and 10.0 wt%, respectively, which is quite far from zero. Hence, it is concluded that the amorphous contents derived from Mo $K\alpha_1$ data are more accurate than those derived from Cu $K\alpha_1$ data. However, it is not possible to reliably quantify amorphous contents below ~8–10 wt% from Mo $K\alpha_1$ and Cu $K\alpha_1$ diffraction data (see Table 3.10.4) with the internal-standard method.

On the contrary, SXRPD reliably allows quantification of amorphous contents down to ~2 wt% for this relatively simple mixture. In addition, the AKLD and the KLD values reported in Table 3.10.4 demonstrate that the synchrotron analyses are indeed much better than the laboratory analyses.

3.10.10. Conclusions

(i) We have thoroughly studied the limit of detection for a well crystallized inorganic phase in an inorganic compound matrix. We have determined the following LoDs for insoluble anhydrite: ~0.2 wt%, ~0.3 wt% and lower than 0.1 wt% for Cu $K\alpha_1$, Mo $K\alpha_1$ and synchrotron radiations, respectively. We conclude that the LoD is slightly better for Cu $K\alpha_1$ than for Mo $K\alpha_1$ because the λ^3 dependence of the diffraction intensity, with similar acquisition times, yielded slightly better signal-to-noise ratios in the Cu patterns. Of course, detector efficiencies also play a role in the measured signal-to-noise ratios.

(ii) We have also studied the limit of quantification for a well crystallized inorganic phase using laboratory X-ray powder diffraction. This phase could be quantified at the level of 0.12 wt% in stable fits with repeatable outputs and good precision. However, the accuracy of these analyses was quite poor, with relative errors close to 100%. Only contents higher than 1.0 wt% yielded analyses with relative errors lower than 20%.

(iii) The Rietveld quantitative phase analysis results from high-resolution Mo $K\alpha_1$ powder diffraction (transmission geometry) and high-resolution Cu $K\alpha_1$ powder diffraction (reflection geometry) were quite similar for a series of crystalline inorganic phase samples. We inferred the validation of the Mo-based analyses procedure from this initial study, as it yielded results very close to well established high-resolution Cu radiation analyses (see Fig. 3.10.7*a*). From the comparison of the AKLD values for the two types of analyses, it was demonstrated that the Mo $K\alpha_1$ analyses were slightly better than those using Cu $K\alpha_1$.

(iv) Comparison of the results obtained from Mo-based and Cu-based patterns for a series of crystalline organic phase mixtures showed that the Mo $K\alpha_1$ analyses gave slightly more accurate values. This conclusion was drawn because the calibration curve obtained from Mo patterns with increasing content of xylose gave an R^2 value closer to 1.0, a slope closer to 1.0 and an intercept value close to 0.0 (see Fig. 3.10.7*b*). The slightly poorer results from Cu $K\alpha_1$ analyses are very likely to be due to the transparency effects in reflection geometry.

(v) Comparison of the results obtained from Mo $K\alpha_1$ and Cu $K\alpha_1$ patterns for a series containing increasing amounts of amorphous glass also indicated that the Mo-based analyses were slightly more accurate than the corresponding Cu $K\alpha_1$ analyses. This conclusion was drawn because the obtained calibration curve from the Mo data has (1) a slope closer to 1.0, (2) a smaller amorphous value for the glass-free sample and (3) a closer agreement between the intercept from the least-squares fit and the determined amorphous value for the glass-free sample (see Fig. 3.10.7*c*). The AKLD analysis confirmed this outcome. Furthermore, the results from synchrotron data have the best accuracy, as shown by the calibration plot and the AKLD analysis.

Finally, we conclude that for the challenging quantification analyses studied here, the results derived from high-energy Mo $K\alpha_1$ patterns were slightly more accurate than those obtained from Cu $K\alpha_1$ patterns. We justify this conclusion based on the larger tested volume for Mo $K\alpha_1$ analyses, which led to better statistics/accuracy in the recorded powder-pattern intensities. The minimization of microabsorption in the Mo $K\alpha_1$ transmission

data is very likely to be an additional factor in the improved accuracy.

This chapter is based on an article *Accuracy in Rietveld quantitative phase analysis: a comparative study of strictly monochromatic Mo and Cu radiations* by León-Reina *et al.* [(2016), *J. Appl. Cryst.* **49**, 722–735]. The work was supported by Spanish MINECO through BIA2014-57658-C2-2-R, which is co-funded by FEDER, and BIA2014-57658-C2-1-R research grants. Funding from Junta de Andalucía (grant P11-FQM-07517) is also acknowledged. We thank CELLS-ALBA (Barcelona, Spain) for providing synchrotron beam time on the BL04-MSPD beamline. All raw powder-diffraction data files underlying this work can be accessed at Zenodo at https://doi.org/10.5281/zenodo.1291900 and used under the Creative Commons Attribution license.

References

Albertsson, J., Abrahams, S. C. & Kvick, Å. (1989). *Atomic displacement, anharmonic thermal vibration, expansivity and pyroelectric coefficient thermal dependences in ZnO. Acta Cryst.* B**45**, 34–40.

Aranda, M. A. G., De la Torre, Á. G. & León-Reina, L. (2012). *Rietveld quantitative phase analysis of OPC clinkers, cements and hydration products. Rev. Mineral. Geochem.* **74**, 169–209.

Bezou, C., Nonat, A., Mutin, J.-C., Christensen, A. N. & Lehmann, M. S. (1995). *Investigation of the crystal structure of γ-$CaSO_4$, $CaSO_4$·0.5H_2O, and $CaSO_4$·0.6H_2O by powder diffraction methods. J. Solid State Chem.* **117**, 165–176.

Brown, G. M. & Levy, H. A. (1979). *α-D-Glucose: further refinement based on neutron-diffraction data. Acta Cryst.* B**35**, 656–659.

Buhrke, V. E., Jenkins, R. & Smith, D. K. (1998). *A Practical Guide for the Preparation of Specimens for X-ray Fluorescence and X-ray Diffraction Analysis.* New York: Wiley.

Cuesta, A., Álvarez-Pinazo, G., García-Maté, M., Santacruz, I., Aranda, M. A. G., De la Torre, Á. G. & León-Reina, L. (2015). *Rietveld quantitative phase analysis with molybdenum radiation. Powder Diffr.* **30**, 25–35.

De La Torre, A. G., Bruque, S. & Aranda, M. A. G. (2001). *Rietveld quantitative amorphous content analysis. J. Appl. Cryst.* **34**, 196–202.

De la Torre, Á. G., López-Olmo, M., Álvarez-Rua, C., García-Granda, S. & Aranda, M. A. G. (2004). *Structure and microstructure of gypsum and its relevance to Rietveld quantitative phase analyses. Powder Diffr.* **19**, 240–246.

Dollase, W. A. (1986). *Correction of intensities for preferred orientation in powder diffractometry: application of the March model. J. Appl. Cryst.* **19**, 267–272.

Egami, T. & Billinge, S. J. L. (2003). *Underneath the Bragg Peaks. Structural Analysis of Complex Materials.* Amsterdam: Pergamon.

Elton, N. J. & Salt, P. D. (1996). *Particle statistics in quantitative X-ray diffractometry. Powder Diffr.* **11**, 218–229.

Fauth, F., Peral, I., Popescu, C. & Knapp, M. (2013). *The new material science powder diffraction beamline at ALBA synchrotron. Powder Diffr.* **28**, S360–S370.

Fries, D. C., Rao, S. T. & Sundaralingam, M. (1971). *Structural chemistry of carbohydrates. III. Crystal and molecular structure of 4-O-β-D-galactopyranosyl-α-D-glucopyranose monohydrate (α-lactose monohydrate). Acta Cryst.* B**27**, 994–1005.

García-Maté, M., Santacruz, I., Cuesta, A., León-Reina, L., Aranda, M. A. G., Baco, I., Morin, V., Walenta, G., Gartner, E. & De la Torre, A. G. (2014). *Amorphous content determination in calcium sulfoaluminate related materials by external and internal standard methodologies. Adv. Cem. Res.* **27**, 417–423.

Garske, D. & Peacor, D. R. (1965). *Refinement of the structure of celestite $SrSO_4$. Z. Kristallogr.* **121**, 204–210.

Hordvik, A. (1971). *The crystal and molecular structure of α-xylose. Acta Chem. Scand.* **25**, 2175–2182.

Kanters, J. A., Roelofsen, G., Alblas, B. P. & Meinders, I. (1977). *The crystal and molecular structure of β-D-fructose, with emphasis on anomeric effect and hydrogen-bond interactions. Acta Cryst.* B**33**, 665–672.

Kirfel, A. & Will, G. (1980). *Charge density in anhydrite, $CaSO_4$, from X-ray and neutron diffraction measurements. Acta Cryst.* B**36**, 2881–2890.

Kullback, S. (1968). *Information Theory and Statistics*, pp. 1–11. New York: Dover.

Larson, A. C. & Von Dreele, R. B. (2000). *General Structure Analysis System (GSAS)*. Los Alamos National Laboratory Report LAUR 86-748.

León-Reina, L., De la Torre, A. G., Porras-Vázquez, J. M., Cruz, M., Ordonez, L. M., Alcobé, X., Gispert-Guirado, F., Larrañaga-Varga, A., Paul, M., Fuellmann, T., Schmidt, R. & Aranda, M. A. G. (2009). *Round robin on Rietveld quantitative phase analysis of Portland cements. J. Appl. Cryst.* **42**, 906–916.

León-Reina, L., García-Maté, M., Álvarez-Pinazo, G., Santacruz, I., Vallcorba, O., De la Torre, A. G. & Aranda, M. A. G. (2016). *Accuracy in Rietveld quantitative phase analysis: a comparative study of strictly monochromatic Mo and Cu radiations. J. Appl. Cryst.* **49**, 722–735.

Madsen, I. C., Scarlett, N. V. Y., Cranswick, L. M. D. & Lwin, T. (2001). *Outcomes of the International Union of Crystallography Commission on Powder Diffraction Round Robin on Quantitative Phase Analysis: samples 1a to 1h. J. Appl. Cryst.* **34**, 409–426.

Madsen, I. C., Scarlett, N. V. Y. & Kern, A. (2011). *Description and survey of methodologies for the determination of amorphous content via X-ray powder diffraction. Z. Kristallogr.* **226**, 944–955.

Maslen, E. N., Streltsov, V. A., Streltsova, N. R. & Ishizawa, N. (1995). *Electron density and optical anisotropy in rhombohedral carbonates. III. Synchrotron X-ray studies of $CaCO_3$, $MgCO_3$ and $MnCO_3$. Acta Cryst.* B**51**, 929–939.

Scarlett, N. V. Y., Madsen, I. C., Cranswick, L. M. D., Lwin, T., Groleau, E., Stephenson, G., Aylmore, M. & Agron-Olshina, N. (2002). *Outcomes of the International Union of Crystallography Commission on Powder Diffraction Round Robin on Quantitative Phase Analysis: samples 2, 3, 4, synthetic bauxite, natural granodiorite and pharmaceuticals. J. Appl. Cryst.* **35**, 383–400.

Stutzman, P. (2005). *Powder diffraction analysis of hydraulic cements: ASTM Rietveld round-robin results on precision. Powder Diffr.* **20**, 97–100.

Thompson, P., Cox, D. E. & Hastings, J. B. (1987). *Rietveld refinement of Debye–Scherrer synchrotron X-ray data from Al_2O_3. J. Appl. Cryst.* **20**, 79–83.

Von Dreele, R. B. & Rodriguez-Carvajal, J. (2008). *Powder Diffraction: Theory and Practice*, edited by R. E. Dinnebier & S. J. L. Billinge, pp. 58–88. Cambridge: Royal Society of Chemistry. https://doi.org/10.1039/9781847558237-00058.

Will, G., Bellotto, M., Parrish, W. & Hart, M. (1988). *Crystal structures of quartz and magnesium germanate by profile analysis of synchrotron-radiation high-resolution powder data. J. Appl. Cryst.* **21**, 182–191.

Zevin, L. S. & Kimmel, G. (1995). *Quantitative X-ray Diffractometry*. New York: Springer-Verlag.